Journal of ELECTRONIC MATERIALS, Vol. 36, No. 8, 2007
DOI: 10.1007/s11664-007-0177-6

High-Performance LWIR MBE-Grown HgCdTe/Si Focal Plane Arrays

RICHARD BORNFREUND,[1,4] JOE P. ROSBECK,[1] YEN N. THAI,[1] EDWARD P. SMITH,[1] DANIEL D. LOFGREEN,[1] MAURO F. VILELA,[1] AIMEE A. BUELL,[1] MICHAEL D. NEWTON,[1] KENNETH KOSAI,[1] SCOTT M. JOHNSON,[2] TERRY J. DELYON,[2] JOHN E. JENSEN,[2] and MEIMEI Z. TIDROW[3]

1.—Raytheon Vision Systems, 75 Coromar Drive, Goleta, CA 93010, USA. 2.—HRL Laboratories, LLC, Malibu, CA, USA. 3.—Missile Defense Agency, Washington, DC, USA. 4.—e-mail: Richard.bornfreund@flir.com

We have been actively pursuing the development of long-wavelength infrared (LWIR) HgCdTe grown by molecular beam epitaxy (MBE) on large-area silicon substrates. The current effort is focused on extending HgCdTe/Si technology to longer wavelengths and lower temperatures. The use of Si versus bulk CdZnTe substrates is being pursued due to the inherent advantages of Si, which include available wafer sizes (as large as 300 mm), lower cost (both for the substrates and number of die per wafer), compatibility with semiconductor processing equipment, and the match of the coefficient of thermal expansion with silicon read-out integrated circuit (ROIC). Raytheon has already demonstrated low-defect, high-quality MBE-grown HgCdTe/Si as large as 150 mm in diameter. The focal plane arrays (FPAs) presented in this paper were grown on 100 mm diameter (211)Si substrates in a Riber Epineat system. The basic device structure is an MBE-grown *p*-on-*n* heterojunction device. Growth begins with a CdTe/ZnTe buffer layer followed by the HgCdTe active device layers; the entire growth process is performed *in situ* to maintain clean interfaces between the various layers. In this experiment the cutoff wavelengths were varied from 10.0 μm to 10.7 μm at 78 K. Detectors with >50% quantum efficiency and R_0A ~1000 Ohms cm^2 were obtained, with 256 × 256, 30 μm focal plane arrays from these detectors demonstrating response operabilities >99%.

Key words: Alternative substrate, silicon substrate, mercury cadmium telluride (HgCdTe), large format, focal plane array (FPA), long-wavelength infrared (LWIR), molecular beam epitaxy (MBE), HgCdTe/Si

INTRODUCTION

Raytheon Vision Systems (RVS) has been a world leader in the development of HgCdTe grown by molecular beam epitaxy (MBE) on silicon substrates.[1,2] High-operability arrays have been demonstrated, culminating in the recent delivery of the first mid-wavelength infrared (MWIR) product arrays for naval research center's (NRL) shipboard distributed aperature systems (DAS) program.[3] The potential advantages for growth by MBE on silicon substrates include the availability of larger substrates (up to 300 mm) at significantly reduced cost compared to CdZnTe substrates (up to 70 × 70 mm^2), the compatibility of round silicon substrates for advanced production semiconductor process equipment, and the thermal matching of the coefficient of thermal expansion of the substrate to the readout integrated circuit (ROIC).

(Received November 27, 2006; accepted January 26, 2007; published online July 12, 2007)

Critical to the production of high-operability arrays is the growth of low-defect, uniform HgCdTe material on the silicon substrates. RVS has demonstrated HgCdTe growth on 150-mm silicon substrates with macrodefect (voids and microvoids) denisty of less than 300 cm^{-2} and composition and thickness uniformities across the 150-mm wafer of less than 1%.[4,5] The HgCdTe multilayer composition profile is controlled by *in situ* spectroscopic ellipsometry (SE) allowing for well-controlled design producibility and material uniformity. In addition, both the buffer layers and HgCdTe layers were grown with the wafer never leaving the vacuum system, eliminating possible material and growth interface degradation induced by exposure to the air.

The HgCdTe device layer design is a *p*-on-*n* heterostructure junction grown on a CdTe/ZnTe buffer layer structure on (211) silicon. All devices in this paper were grown on 4-in. silicon wafers in a Riber Epineat 5-in. MBE system. RVS has both this 5-in. MBE system as well as a 10-in.-capable VG V100 MBE system.

Despite the excellent MWIR results, there have been questions as to the ability of longer-wavelength material with detector cutoffs >10 μm to have low enough leakage currents (or high enough R_0A) to support useful applications. This paper describes the current state of LWIR HgCdTe/Si at Raytheon Vision Systems, in which second-generation quality LWIR material with >10 μm cutoffs at 78 K have been processed into FPAs with excellent performance, demonstrating the feasibility of LWIR HgCdTe/Si FPAs.

The layer designs used are based on earlier MWIR designs shown in Fig. 1. The detector design includes a partial pixel delineation and indium bumps are used for the interconnection of the detector pixel to the ROIC pixel. This design matches the design used on our high-operability MWIR FPAs grown on silicon substrates and represented a starting point for evaluation of long-wavelength performance.

LWIR development effort is part of a multiyear program to extend the cutoff wavelength of the HgCdTe/Si FPAs. The first half of the program is to provide an initial baseline LWIR FPA performance utilizing the 256×256, 30 μm FPA format for detector $\lambda_{50\%}$ = 10 μm at 78 K. During the latter portion of the program, the detector performance will be evaluated for extending the $\lambda_{50\%}$ = 10.5 μm at 78 K using both 256×256, 30 μm and 640×480, 20 μm FPA formats.

ALTERNATIVE SUBSTRATE GROWTH

Epitaxial growth of any material onto lattice-mismatched substrates is always a challenge. Infrared materials add the additional complication of small band-gaps, which are more sensitive to the presence of material strains and growth defects. The major areas of concern include:

- Layer compositional control and uniformity
- Crystal defects
- Crystallographic orientation
- Interface quality.

The general layer design is shown in Fig. 1. Layer compositional control and uniformity are generic MBE growth issues that are controlled predominantly by the system chamber and source designs. Temperature uniformity across the substrate during growth plays a significant role in the compositional uniformity of the epitaxial layers. The compositional dependence of HgCdTe on the cutoff wavelength of the material is greater for LWIR material, requiring more-precise control of temperature uniformity to maximize wafer yield.

The interface quality plays a critical role in both the crystal quality and minimizing the presence of growth defects. The initial substrate preparation both prior to insertion into the MBE system and after insertion into the chamber determine substrate quality and eventual detector yield. We believe that the *in situ* growth of both the buffer layers and infrared active HgCdTe layers without subjecting the wafers to the outside of the vacuum system is necessary for achieving consistently low-defect wafers.

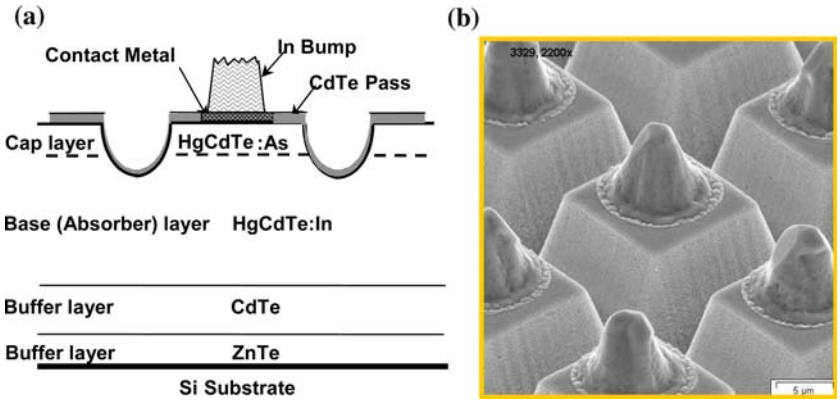

Fig. 1. (a) Cross section of the MBE-grown heterojunction layer design, and (b) an example processed detector.

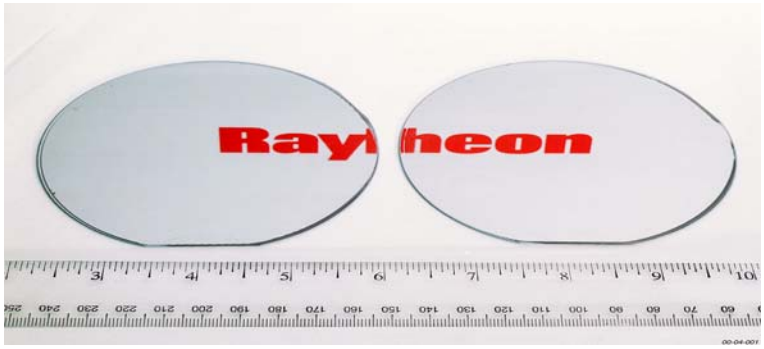

Fig. 2. Example of HgCdTe film quality grown on 4-in. silicon alternative substrates.

As with other material systems, buffer layers are necessary to accommodate the lattice mismatch between the growth substrate and HgCdTe layers. To date, the CdTe/ZnTe buffer system has represented the best results. The ZnTe layer controls the crystallographic orientation as well as providing an incremental step in lattice constant. The CdTe layer further steps the lattice constant differences. An example of the final film quality is shown in Fig. 2.

DETECTOR WAFER PERFORMANCE

The five 4-in. wafers examined in this study had 78 K 50% cutoffs (per photon) between 10 μm and 10.7 μm at 78 K. Test structure assemblies (TSAs) were processed on the wafer along with the detector arrays and examined to provide direct material performance data. As will be shown from the FPA performance, the spectral and quantum efficiency (QE) performance of the detector material was excellent, with non-antireflection (AR)-coated quantum efficiencies >50% for four out of the five wafers. Table I summarizes the cutoffs and quantum efficiencies of the wafers examined. The QE meaurements were performed using a 6.5-μm spike filter.

Figure 3a shows the R_0A versus 1000/T curve for both 30 μm × 30 μm and 40 μm × 40 μm diodes from wafer 1. The wafer shows diffusion-limited behavior down to about 65 K with a changeover to a temperature slope more consistent with tunneling behavior. While the majority of pixels displayed consistent performance, one device demonstrates a lower breakover point, illustrating the areas where improved understanding is required for this material system. Figure 3b shows a representative relative spectral response measured on wafer 3 at 78 K. The pixel geometry measured 30 μm × 30 μm. The pixels tested all show consistent response characteristics and well-behaved spectrals. Figure 4 illustrates the I-V curves for 30 μm × 30 μm diodes measured at 78 K under zero field of view (0FOV) conditions. The I-V curves show good repeatibility, with breakdowns >100 mV for LWIR material and saturation currents ~10–20 pA.

Table I. Detector Wafer Summary for Long-Wavelength (LW) HgCdTe/Si Detector Characteristics. The QE Measurements were Performed on Non-Antireflection-Coated Test Structure Assemblies

Wafer	Wafer	78 K 50% Cutoff/Photon	QE (%)
1	3–1608	9.7	49
2	3–2045	10.7	53
3	3–2043	10.1	57
4	3–2049	10.4	63
5	3–2050	10.0	67

FOCAL PLANE ARRAY PERFORMANCE

The application of the LWIR HgCdTe/Si detectors is for imaging, typically around 10^{15} ph/cm^2-s to 10^{16} ph/cm^2-s flux levels. While test structure data is a useful indicator for median detector performance, they are of limited statistical significance. A better statistical indicator of detector performance is the assembly and testing of focal planes arrays (FPA). The rest of this section will present FPA data and the resulting image quality of 256 × 256, 30 μm format arrays.

FPA Test Conditions

Evaluation of the LWIR detector material performance was performed using the SB172 readout integrated circuit (ROIC). The SB172 is a 256 × 256, 30 μm format ROIC, with the capability of operating in a two-color sequential mode with snapshot integration up to a 120 Hz frame rate. The charge capacity of the ROIC is 31 Me$^-$ with the unit cell of the ROIC containing a direct injection circuit. The minimum operating temperature is 60 K. A picture of an FPA mounted in a leadless chip carrier is shown in Fig. 5.

The FPAs were initially screen tested under the test conditions summarized in Table II at F/5.5 and 78 K. All of the FPAs were evaluated for operability using the same requirements. All active array pixels were included in the evaluation. For the cases where an engineering ROIC with a known defective

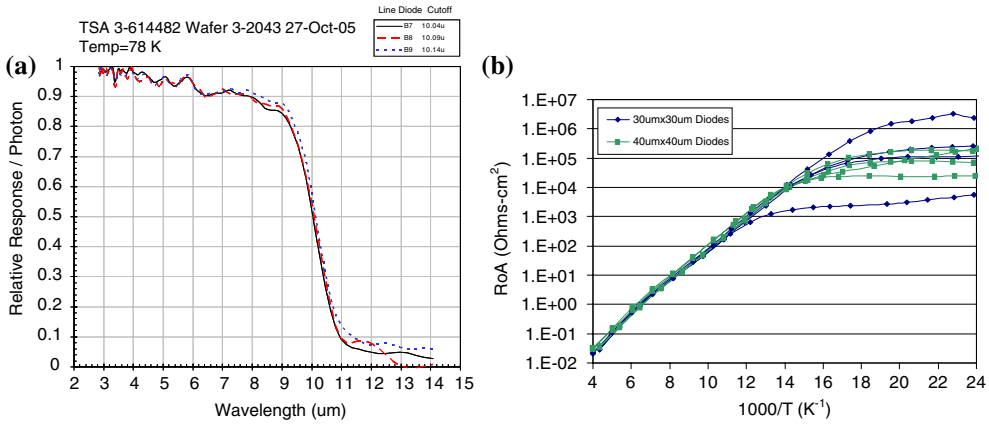

Fig. 3. Detector performance: (a) 30 μm $\times$ 30 μm diode I_0A versus $1/T$ behavior from wafer 1. Diffusion-limited performance is observed down to ~65 K; (b) relative spectral response of wafer 3 measured at 78 K. This wafer had a 50% cutoff of 10.1 μm. The detector pixel dimensions were 30 μm $\times$ 30 μm.

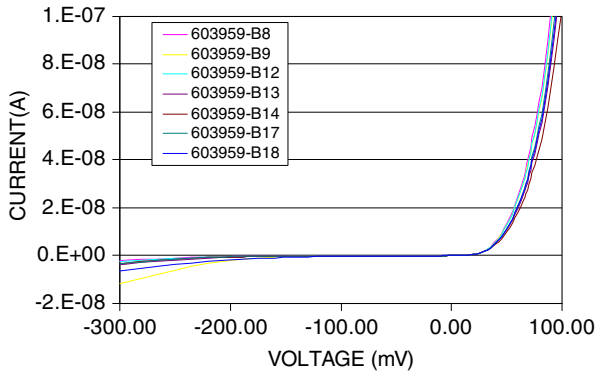

Fig. 4. Detector performance: *I-V* performance of 30 μm $\times$ 30 μm detector diodes measured at 78 K under 0FOV.

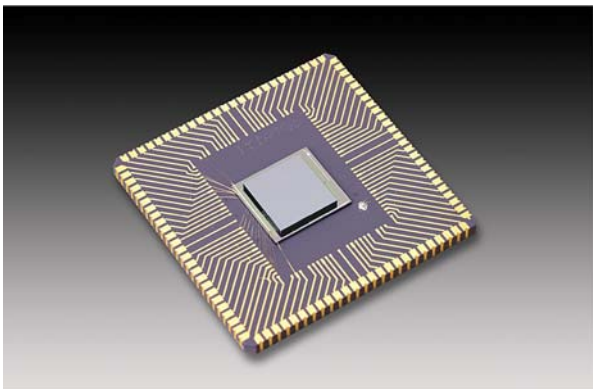

Fig. 5. LWIR HgCdTe/Si 256 $\times$ 256 array (30-μm unit cell) hybridized to a SB172 ROIC. The FPA is shown mounted in a leadless chip carrier.

row or column outage was used, the defective row/column was not included in the statistics. The response operability was based on any pixel between half and one and a half of the mean array response, consistent with tactical program operability definitions such as the dual-band focal-plane manufacturing M/L program currently being pursued at RVS and night vision and electronics sensors directorate (NVESD). The noise equivalent temperature difference (NETD) operability was derived using a requirement for the pixel being more than zero and less than twice the median NETD for the array. The lower limit is included in the operability to discount pixels with deceptively low values of NETD, which are in fact nonoperable. The net array operability includes both the response and NETD operabilities.

Table II. Test Conditions for the SB172 256 $\times$ 256 LW HgCdTe/Si FPAs. All of the FPAs were Tested at *F*/5.5, While FPA 615165 was Tested at *F*/5.5

Test Parameter	Value
Operating Temperature	78 K
F#	5.5
Blackbody Temperatures	350 K, 360 K
IR Bandpass	6.1–7.9 μm
Integration Time	1.5 ms

FPA Test Results at *F*/5.5 and 78 K

The FPAs results demonstrate some of the best LWIR performance ever measured for LWIR HgCdTe/Si detectors. Near second-generation performance was obtained and is summarized in Table III. Response operabilities >99% were obtained for FPAs tested under tactical flux conditions for four of the nine parts. The parts encompass detector wafers from multiple process lots and five different detector wafers. The general quality of the FPAs from multiple wafer/process lots indicates the potential reproducibility of the growth and wafer production processes. A detailed examination of the FPA performance at 78 K and *F*/5.5 is included for FPA 615165 as shown in Fig. 6. The responsivity

Table III. Summary of 78 K FPA Data Measured Under *F*/5.5 Test Conditions Demonstrating the Excellent FPA Performance. The Details of the Operability Definitions are Contained in Section 2.1

FPA ID	Wafer	50% Cutoff @ 78 K	Median Resp* mV/K	Res Sig./Mean (%) (Op. Pixels Only)	Median NETD mK	Row/Col. Out	0.5–1.5 Resp. Op. (%)	< 2* Median NETD Op. (%)	Net Oper. (%)
614300	1	9.7	22.1	7.6	23.7	1	98.9	95.4	95.4
614477	2	10.7	19.6	10.2	34.2	1	92.6	80.0	79.9
614478	2	10.7	12.5	12.0	65.8	1	95.3	83.1	83.0
614479	3	10.1	20.5	6.7	27.7	1	99.3	92.0	92.0
614480	3	10.1	20.4	8.5	27.9	1	99.0	90.1	90.1
615162	4	10.4	15.7	16.2	50.5	0	96.7	91.0	90.8
615163	4	10.4	14.9	15.4	44.4	0	93.4	77.5	77.4
615164	5	10.0	21.2	6.8	26.9	0	99.0	87.2	87.1
615165	5	10.0	22.3	6.2	24.3	0	99.6	94.2	94.2

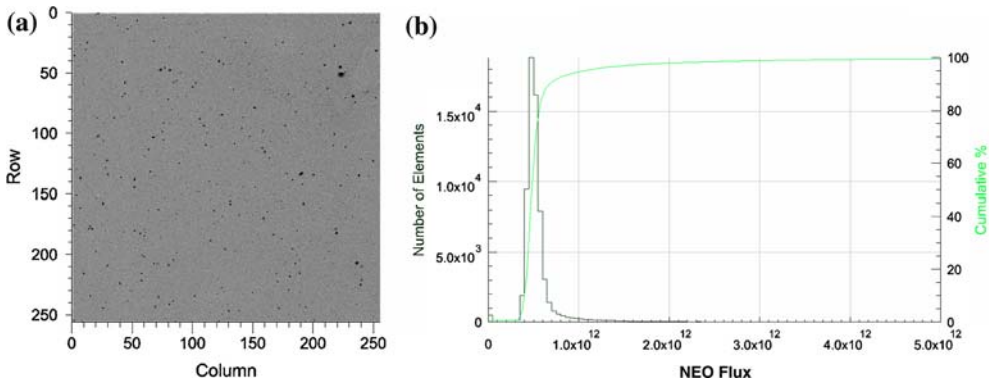

Fig. 6. Performance of FPA 615165 at a temperature of 78 K and *F*/5.5. (a) A response greyscale illustrating the quality of the detector. The response operability for a 3:1 window is 99.6%, with (b) showing the noise equivalent irradiance (NEI) histogram. The median NEI of the FPA is 5.87×10^{11} ph/cm^2-s.

value of 23 mV/K is consistent with a non-AR-coated quantum efficiency >50%, while the median NETD value of 24 mK is consistent with an R_0A value ~10^3 $\Omega \cdot \text{cm}^2$ for a cutoff wavelength of 10.1 μm. A more-detailed look at the effective R_0A value measured at 0FOV on the FPA is presented in Section 3.4. The response operability for this part obtained under *F*/5.5 testing was 99.6%. The NETD operability was 92% with the net operability also approximately 92%, illustrating that the operability limitations are predominantly due to the NETD. Given the relatively tight distribution of pixel response, this result is consistent with the presence of a noise tail.

Leakage Current Behavior at 78 K

The dominant limiting factor in LWIR detectors is the higher leakage current as a result of the associated smaller material band gaps and material defects. The presence of elevated etch pit densities (EPD) in HgCdTe/CdZnTe has in the past been shown to increase the detector dark current of the material.[6] Since HgCdTe/Si materials have higher EPD levels, it is important to understand if this limits the dark current performance in the FPAs.

Figure 7 shows the 0FOV offset measurements as a function of the integration time for one of the FPAs and the effective R_0A values derived from the slope of the line. The offset change with integration time is very linear, allowing for an excellent linear fit of the data as shown in Fig. 7a. Both the median and mean direct-current (DC) offsets are shown. The higher slope for the mean values is consistent with the existence of a small tail of higher leakage current pixels. The effective R_0A is derived from the slope by the relation:

$$R_0A \sim \frac{kTZA_{\text{opt}}}{e^2m}$$

where k = Boltzman's constant, T = operating temperature of the device, Z = transimpedance of the ROIC (in V/e), A_{opt} = optical area of the detector pixel, e = electronic charge, and m = slope of the DC offset versus integration time.

The derived R_0A values are segregated by the detector wafer and show the consistency of the measurement for each wafer. Wafers 2 through 5 each had two FPAs tested. As expected, the lower-R_0A wafers demonstrated higher NETD values due the associated higher leakage currents. To gauge

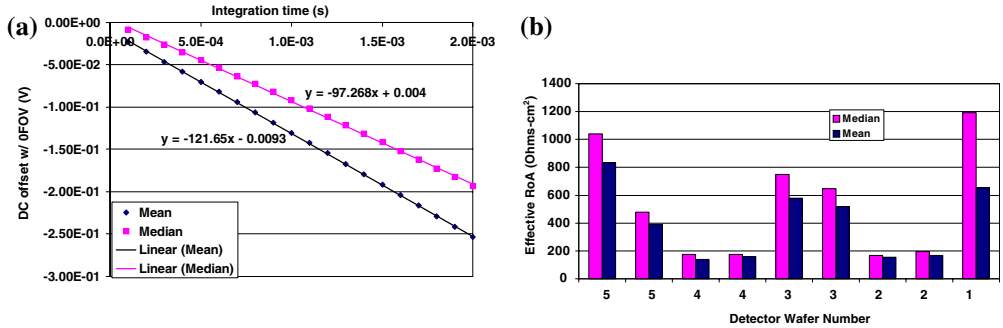

Fig. 7. Results of 0FOV measurements on the FPA: (a) the measured DC offset for one of the FPAs is shown and demonstrates a very linear dependence of offset with integration time. Both the mean and median offsets are shown; (b) the effective R_0A derived from the slope of the DC offsets and are consistent with the FPA noise levels.

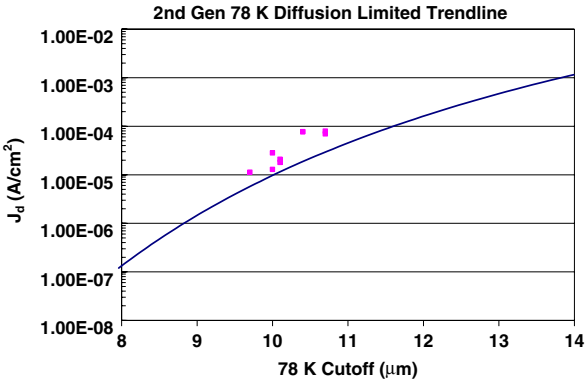

Fig. 8. Leakage current densities of the FPAs measured under 0FOV conditions compared to the current second-generation diffusion-limited trendline for 78 K.

the quality of the parts truly, the measured 0FOV leakage current densities were compared to the current second-generation 78 K diffusion-limited trendline, illustrating the LPE-grown HgCdTe/CdZnTe performance as shown in Fig. 8. While further work is needed to continue to improve the performance of the HgCdTe/Si, the near-trendline quality of the material shows excellent potential for matching HgCdTe/CdZnTe performance.

Imaging Performance of the HgCdTe/Si FPAs

The ultimate indicator for the use of a detector material is the ability to image objects as part of an optical system. For this purpose, a highly uniform response with low noise levels is desired. Figure 9 shows two images taken under different flux conditions. Figure 9 contains both an image taken in a dark room while the second image was taken under daylight conditions. Both images show excellent sensitivity with clear definition of both objects up close (a) and objects in the distance (b). The imaging was performed at $F/2.3$ at 78 K.

SUMMARY

Raytheon Vision Systems has demonstrated state-of-the-art performance for LWIR HgCdTe grown by molecular beam epitaxy on silicon substrates. Wafers with cutoffs varying from 10.0 μm to 10.7 μm have been grown on 4-in. silicon wafers and processed into 256×256, 30 μm pitch FPAs. Operabilities as high as 99.6% for the response operability have been measured, with four out of the nine FPAs achieving >99% response operability to a 0.5–1.5 response specification. Responsivities at 78 K were as high as 22 mV/K and NETDs as low as 24 mK consistent with a non-AR-coated quantum efficiencies >50% were measured. The NETD levels are consistent with effective R_0A values of approximately 1,000 $\Omega \cdot \text{cm}^2$ determined from 0FOV measurements at 78 K.

The quality of the FPAs allows for high-sensitivity imagery with few material defects. The excellent performance of the FPAs demonstrates the feasi-

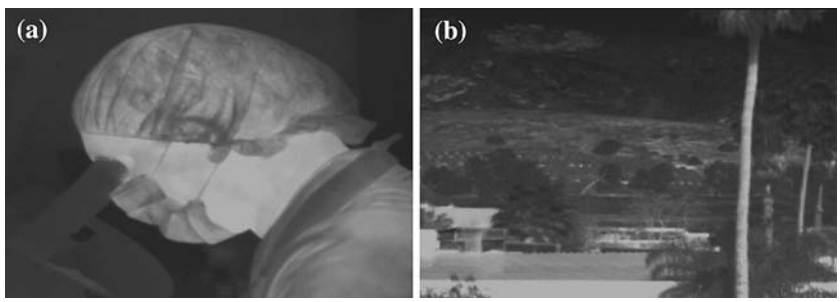

Fig. 9. Images from FPA 615165 taken under different imaging conditions: (a) an indoor image at a lower flux level, and (b) an image taken under daylight conditions. The temperature of the FPA was 78 K.

bility of extending MBE-grown HgCdTe on silicon to cutoff wavelengths greater than 10 μm and the potential for insertion into imaging systems. The results demonstrate the promise of LWIR HgCdTe on silicon detectors and illustrate the areas of focus to continue to improve the FPA performance.

ACKNOWLEDGEMENTS

Work supported by the Missile Defense Agency (MDA) through CACI Technologies, Inc. subcontract no. 601-05-0088, NVESD technical task order no. TTO-01, prime contract no. DAAB07-03-D-C214, (delivery order no. 0016).

REFERENCES

1. K.D. Maranowski, J.M. Peterson, S.M. Johnson, J.B. Varesi, W.A. Radford, A.C. Childs, R.E. Bornfreund, and A.A. Buell, *J. Electron. Mater.* 30, 619 (2001).
2. J.M. Peterson, J.A Franklin, M. Reddy, S.M. Johnson, E. Smith, W.A. Radford, and I. Kasai, *J. Electron. Mater.* 35, 1283 (2006).
3. D.J. Gulbransen, S.H. Black, A.C. Childs, C.L. Fletcher, S.M. Johnson, W.A. Radford, G.M. Venzor, J.P. Sienicki, A.D. Thompson, J.H. Griffith, A.A. Buell, M.F. Vilela, M.D. Newton, E. Takken, J. Waterman, and K. Krapels, *Proc. SPIE* 5406, 305 (2004).
4. S.M. Johnson, W.A. Radford, A.A Buell, M.F. Vilela, J.M. Peterson, J.J. Franklin, R.E. Bornfreund, A.C. Childs, G.M. Venzor, M.D. Newton, E.P. Smith, L.M. Ruzicka, G.K. Pierce, D.D. Lofgreen, T.J. Lyon, and J.J. Jensen, *Proc. SPIE* 5732, 250 (2005).
5. N.K. Dhar and M.Z. Tidrow, *Proc. SPIE* 5564, 34 (2004).
6. S.M. Johnson, D.R. Rhiger, J.P. Rosbeck, J.M. Petersen, S.M. Taylor, and M.E. Boyd, *J. Vac. Sci. Technol. B* 10, 1499 (1992).